UNIVERSITY OF OKLAHOMA

GRADUATE COLLEGE

QUANTIFYING NANOPARTICLE ATTACHMENT TO PRODUCE SURFACES

A THESIS

SUBMITTED TO THE GRADUATE FACULTY

in partial fulfillment of the requirements for the

Degree of

MASTER OF SCIENCE

By

JACK BEZDEK

Norman, Oklahoma

2024

QUANTIFYING NANOPARTICLE ATTACHMENT TO PRODUCE SURFACES

A THESIS APPROVED FOR THE

SCHOOL OF CIVIL ENGINEERING AND ENVIRONMENTAL SCIENCE

BY THE COMMITTEE CONSISTING OF

Dr. Tohren Kibbey, Chair

Dr. Keith Strevett

Dr. Kendra Dresback

DEDICATION

This work is dedicated to my parents, Greg and Debra Bezdek, who offered surprisingly little resistance when I told them I was considering grad school.

ACKNOWLEDGEMENTS

This work was supported by the USDA National Institute of Food and Agriculture through Agriculture and Food Research Initiative (AFRI) grant number 2020-65210-30765. It would not have been possible without the guidance of my advisor, Dr. Tohren Kibbey, as well as my co-chair Dr. Keith Strevett and committee member Dr. Kendra Dresback. Their expertise and leadership have guided me throughout the development of this thesis. I would also like to thank Elina Avila and Nour Alfailakawi for their assistance in laboratory work. Finally, Dr. Preston Larson's microscopy work was invaluable for the latter half of this thesis.

TABLE OF CONTENTS

LIST OF TABLES

LIST OF FIGURES

ABSTRACT

In recent years, nanoparticles have emerged as an intriguing tool in the field of agriculture, showing capabilities to increase performance and efficiency in several areas throughout the process of crop production. For many applications, their beneficial abilities depend on their resistance to detachment. However, this quality can have detrimental effects to human health once produce has left the farm. Therefore, it is important to accurately quantify attachment and detachment, as well as provide insight into what factors influence these qualities. Nanoparticles of different structure and concentration were applied to organic surfaces in 5 μL drops. A rinsing procedure was then developed to simulate a process by which produce is washed before consumption. Samples were then imaged with a scanning electron microscope (SEM) using both backscatter and secondary electron modes. Using the SEM's backscatter electron detection, an image thresholding program was developed. Images were broken into pixels and segmented by brightness intensity. A threshold was then calculated from the derivative of reverse-cumulative brightness intensity frequency, from which pixels were binned into nanoparticles and non-nanoparticles. Images were taken of both rinsed and unrinsed surfaces, allowing a visual comparison and computerized quantification of detachment rates. At higher nanoparticle concentrations, significant detachment took place for nanoparticles studied. No decrease in particle frequency could be observed at the low end of concentrations. Addition of extracellular polymeric substances (EPS) as well as variations in pH had no observed significant effect on detachment.

1. INTRODUCTION

As the global population continues to increase, one looming challenge is the adaptation of agriculture to feed an ever-growing number of people. Nanoparticles have become a frequent aid in the fight against world hunger. Introduced in all phases of the farm-to-shelf process, nanoparticles have been shown to be effective in warding off pests, supplying nutrients, and recognizing mineral deficiency (Mittal et al., 2020). Zinc oxide and titanium dioxide are two such nanoparticles with agricultural applications, with the latter demonstrating abilities to elevate nitrate efficiency and increase disinfectant potential. (Dekkers et al., 2011; Krishna et al., 2005). Despite their use, these nanoparticles are effective in many applications only as long as they can adhere to produce surfaces and withstand natural perturbations such as wind and rain.

While nanoparticles have the potential to provide benefits in agriculture, their ability to adhere to produce surfaces can be a detriment long after their usefulness has ceased. The bounds of a nanoparticle's size are not fully agreed upon, with different sources setting an upper limit at 100, 500, and 1000 nm (Aschner, 2009; Medina et al., 2007; Powers et al., 2006). Regardless of their exact definition, their fineness could have damaging effects. Recent studies of fine particles have demonstrated their capabilities to negatively affect human health (Kannan & Vimalkumar, 2021; Lu et al., 2022; Vianello et al., 2019). Nanoparticle consumption raises similar concerns with an ability to penetrate deep within the human body as well as relocate into unintended regions of crops (Ji et al., 2011; Roohinejad & Greiner, 2016). With nanoparticles' notable positive and negative consequences, it is important to be able to quantify their attachment to produce surfaces, as well as understand the factors that influence it.

The work presented here studied the attachment of zinc oxide and titanium dioxide nanoparticles to spinach-related surfaces, including fresh leaves, rotten leaves, leaves with extracellular polymeric substances (EPS), and EPS alone. A rinsing procedure was developed to enable a comparison of samples before and after immersion in a water bath. The samples were then imaged in a scanning electron microscope (SEM) in a method which enabled future quantification without allowing it to be damaged through the microscope's vacuum. Finally, the images were analyzed using thresholding computer analysis to quantify the initial and remaining coverage of nanoparticles. The results were evaluated in the context of nanoparticle properties.

2. LITERATURE REVIEW

2.1 Properties of Zinc Oxide

Zinc's stature as an essential component of agriculture has been known for decades. The element is found naturally in soils, but critically low levels in semi-arid regions present risks to major food staples like rice and wheat (Tulchinsky, 2010). In the United States, zinc deficiencies once found in Great Plains states have been mostly eradicated through high use of zinc fertilizers (Takkar & Walker, 1993). Various zinc compounds have been used to enrich soil, with zinc oxide joining zinc nitrate, zinc chloride, and zinc sulphate, the latter being the most used (Mortvedt & Gilkes, 1993). Zinc oxide's differences with the popular zinc sulfate lie in several areas, with that most relevant to this study being their water solubility. Zinc sulfate is highly soluble (98%), which early studies considered necessary for correcting zinc deficiency in crops. However, newer studies conclude that highly insoluble compounds such as zinc oxide (Solubility = 0.0004%) are equally effective in correcting deficiency, although zinc oxide must be added in higher amounts (Shivay et al., 2008).

Several efforts have justified the use of the insoluble zinc oxide as a beneficial fertilizer. One study found that soil enriched with zinc oxide nanoparticles increased a wheat crop's chlorophyll A and B contents, plant height at vegetative and maturity stages, shoot and spike lengths, and fresh and dry root weights, particularly under salt-stressed conditions (Adil et al., 2022). Another study focusing on rice found that the introduction of zinc oxide nanoparticles led to higher yield, increased production quality, and even an improvement in taste through a reduction in kernel breakage. However, it was observed that particularly high levels led to an increase in chalkiness (Mi et al., 2023). Other researchers have found similar concerns with

excess zinc oxide in agriculture, including an induction of toxicity in soil and reduction in microbial biomass carbon (Shemawar et al., 2021). Though research has been done on the side effects of zinc oxide introduction for plant life, little information exists regarding the carryover of zinc oxide from a crop site to a consumer's table.

2.2 Properties of Titanium Dioxide

Titanium dioxide is another nanoparticle with extensive uses in agriculture. Unlike zinc, titanium is not an essential trace element, meaning titanium dioxide is not a necessary component of soil for nutritional purposes. Nevertheless, application of nano titanium dioxide has been shown to increase essential oil content and decrease hydrogen peroxide content in crops, mitigating the harmful effects of high salinity (Gohari et al., 2020). Another study found that spinach had increased levels of chlorophyll and several beneficial enzymes after exposure to anatase, a mineral form of titanium dioxide (Lei et al., 2008). As with zinc oxide, the use of titanium dioxide in high concentrations has been observed to have toxic side effects. Consequences of titanium dioxide attachment include degradation of cell walls and cell membranes, leading to adhesion to intracellular organelles and macromolecules (Hou et al., 2019). As with zinc oxide, studies in titanium dioxide application have focused primarily on behavior at the crop site.

2.3 Theories and Factors Influencing Particle Attachment

Derjaguin-Landau-Verwey-Overbeek (DLVO) theory has long been a tool for measuring attachment of liquid suspensions. Established in the 1940s, DLVO theory describes a suspension's attraction to a surface as a combination of electrostatic and van der Waals forces (Derjaguin & Landau, 1993; Verwey, 1947). The likelihood of attachment is related to the ionic

strength of the solution and separation distance of the surfaces. However, modern review of this theory suggests electrostatic and van der Waals forces alone only show a full picture for a limited range of surfaces. Extended DLVO (xDLVO) theory builds on DLVO theory by adding acid-base interaction force to electrostatic and van der Waals forces (van Oss, 1993). Measuring the sum of these three forces over surface separation reveals the attractive or repulsive tendencies between two surfaces. In some cases, at distances further than a critical value, repulsive electrostatic forces dominate over the other two, culminating in an maximum repulsion at an "energy barrier" (Liu et al., 2021). However, at closer distances, an increase in attractive and highly sensitive to distance van der Waals forces (and often acid-base forces) overpower electrostatic forces, eventually creating a net attractive force. One important output of xDLVO theory is the value of this energy barrier. At certain ionic strengths, this repulsive force is so high as to prevent any possible crossing of this threshold (Adair, Suvaci, & Sindel, 2001). Several surface and particle factors influence the value of this energy barrier and strength of the resultant attraction, including particle size and zeta potential. Zeta potential – a measure of surface charge – is a factor of particular interest due to its ease of measurement and direct relation to surface attachment.

Zeta potential is a measurement of electric potential at the boundary surrounding a particle at which ions are no longer firmly bound to it. The magnitude of zeta potential can describe the stability of a dispersion. In theory, a high value promotes a repulsive force between particles and allows little potential for attraction (Hunter, 1989). Laboratory studies of this effect have corroborated that an increase in absolute zeta potential can decrease attachment efficiency and, in turn, increase repulsive electrostatic forces (Liu et al., 2021).

2.4 Relevant Experiments in Nanoparticle Quantification

Other studies have dealt with the matter of quantifying nanoparticles attached to a surface. Many include some form of automatic image thresholding, though each vary slightly in their techniques (Dai et al., 2018; Sheth et al., 2023; Wang, 2016). While some established thresholding procedures have been designed to identify one nanoparticle type only, others can adjust their thresholds to accommodate several different nanoparticles (Ilett et al., 2020; Shvedchenko & Suvorova, 2017).

3. METHODOLOGIES

3.1 Rinsing Procedures

Two powders containing nanoparticles (nanopowders) were obtained for this work: titanium dioxide (TiO_2) obtained from Degussa Corporation (Düsseldorf, Germany) and zinc oxide (ZnO) obtained from Sigma-Aldrich (St. Louis, United States). In addition to their agricultural benefits, zinc oxide was selected for its high molecular weight, promoting firm attachment to the spinach surface, while titanium dioxide was selected for its consistent cluster formation, allowing for a greater ability to discern nanoparticles from other matter remaining on the surface. Both nanopowders were used as purchased.

Baby spinach (*Spinacia oleracea*) was purchased from a local retailer and refrigerated until the morning of use, typically removed about three hours before imaging. Upon transportation to the rinsing laboratory, leaves with satisfactory criteria were identified and separated from those remaining. Criteria included abaxial sides (undersides) particularly free of blemishes, sizable gaps between veins to ensure a smooth topography under the nanopowder droplet, and sturdy petioles (stalks) to support the removal of leaves from the rinsing solution. The selected leaves were then subject to an initial rinse of deionized (DI) water before being allowed to dry with the abaxial side facing upward. During this drying process, two resources were created: the nanopowder suspension, to be dropped onto the leaf surface, and the rinsing solution, in which the leaf was to be partially submerged.

Two concentrations of nanopowders were used for their suspensions: 20 mg/L and 200 mg/L, each with similar procedures of creation. In both cases, the nanopowder of interest was weighed and added to a borosilicate glass volumetric flask. Then, 250 mL of DI water were

added to the flask. After 30 seconds atop a stirrer, the suspension was transferred to a polypropylene tube to allow for safe sonication with a wand sonicator (ultrasonic processor, Cole-Parmer, Vernon Hills, IL). As with the nanopowder suspensions, the rinsing solutions were created by weighing 1.5 mg sodium chloride into a 250 mL volumetric flask and diluting with water, resulting in a concentration of 10^{-4} M. The solutions were then stirred for 30 seconds and stored at room temperature. To study the effects of pH on nanoparticle detachment, a high-pH rinsing solution was also created. A 250 mg quantity of the original rinsing solution was procured. 10 mg of sodium hydroxide were then added to the solution, resulting in a molarity of 10^{-3}. To further dilute the solution, 250 µL were pipetted from the flask and added to a separate 250 mL flask of the original rinsing solution, culminating in a molarity of 10^{-6}. The remaining intermediary solution was then deposited into waste containers. As in the neutral solution, the high-pH solution was then stirred for 30 seconds and stored at room temperature. The new solution was measured to have a pH of 8.35, considerably higher than the original, neutral-pH solution, measured at 6.02.

Once the leaves had dried from the initial rinse, it was necessary to mark the regions in which the nanopowder suspension was to be dropped (henceforth called “regions”). Without marking, regions were difficult to locate in SEM images after drying. This was originally performed by using fine marker directly onto the leaf surface, either drawing a ring approximately ½ inch in diameter or an arrow in the direction of the region However, contact between the marker and leaf was found to damage surrounding cells and affect the structure of the region. The process was then modified to include pieces of ring-shaped tape applied to non-veinous sections of their abaxial sides, encircling a region 5 mm in diameter. The original and modified methods of marking are seen in Figure 1.A and 1.B, respectively. The selected

nanopowder suspension was then sonicated at 21% power for 60 seconds. Using a micropipette, a 5 µL droplet of the suspension was placed onto the center of each circular region, after which each leaf was again allowed to dry. Once dry, the rinsing solution was stirred for an additional 30 seconds and placed into rinsing beakers with a depth of approximately one inch. Each leaf was then placed vertically into a beaker with the petiole facing upward. With this setup, one region (the "far region") was submerged in the rinsing solution while all other regions remained above liquid level. This procedure is denoted as the "final rinse." Once in this state for 60 seconds, the leaves were removed from their beakers and once again allowed to dry at room temperature with their abaxial sides facing upward.

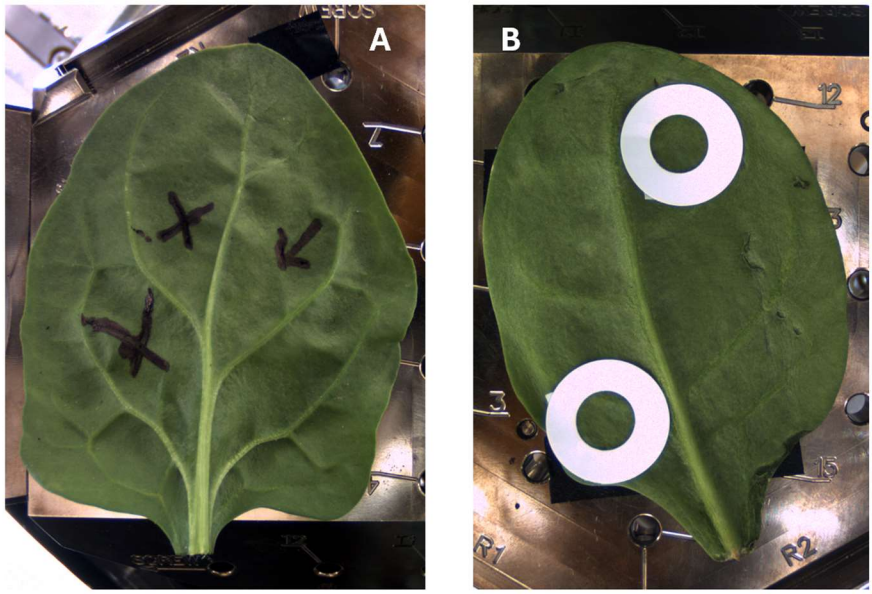

Figure 1. Two methods of marking regions on fresh leaves: (A) using marker, and (B) using ring-shaped tape

In addition to dry, fresh leaves, the rinsing and imaging experiments were also performed on rotten leaves, as well as fresh leaves covered in a layer of extracellular polymeric substances (EPS). The rotten leaves were procured by leaving a container of fresh leaves in a refrigerator

over a period of five weeks, after which leaves with visible rot but structural integrity were selected. Even with this selection procedure, the lack of rigidity of the selected leaves necessitated a slightly modified final rinse procedure. Unlike fresh samples, an attempt to submerge a rotten leaf would typically result in the tip (the point of the leaf furthest from the petiole) remaining buoyant, preventing the far region from breaking through the rinsing solution's surface. To combat this, continuous pressure was applied to the tip to submerge it vertically against the beaker wall, leaving the far region in a position like that of fresh leaves. This pressure was applied for the duration of the final rinse, being lifted when it was time to remove the rotten leaf from the beaker for drying. To obtain EPS, a container of fresh leaves was left in a non-refrigerated, humid setting over four weeks. After this period, the liquid secretions were drained from the rotten leaves into a glass container and refrigerated. Varying techniques were used to add these secretions (EPS) to fresh leaves, shown in Figure 2. In one technique, 3 mL of EPS were pipetted onto level regions of the leaf surface and allowed to dry, resulting in apparent circular regions. In another technique, the EPS container would be poured over the leaf, creating a similarly thick yet more widespread layer of EPS on the leaf surface. Finally, one technique saw a leaf dipped and pressed into the EPS container, creating a thin layer of EPS on the entire abaxial surface. For the latter two techniques, tape had to be applied to mark a region in which the nanopowder suspension would be dropped. For the former, the dried EPS served the function of the tape, clearly marking a region. For all experiments with EPS on leaves, the final rinse procedure was identical to that of dry, fresh leaves.

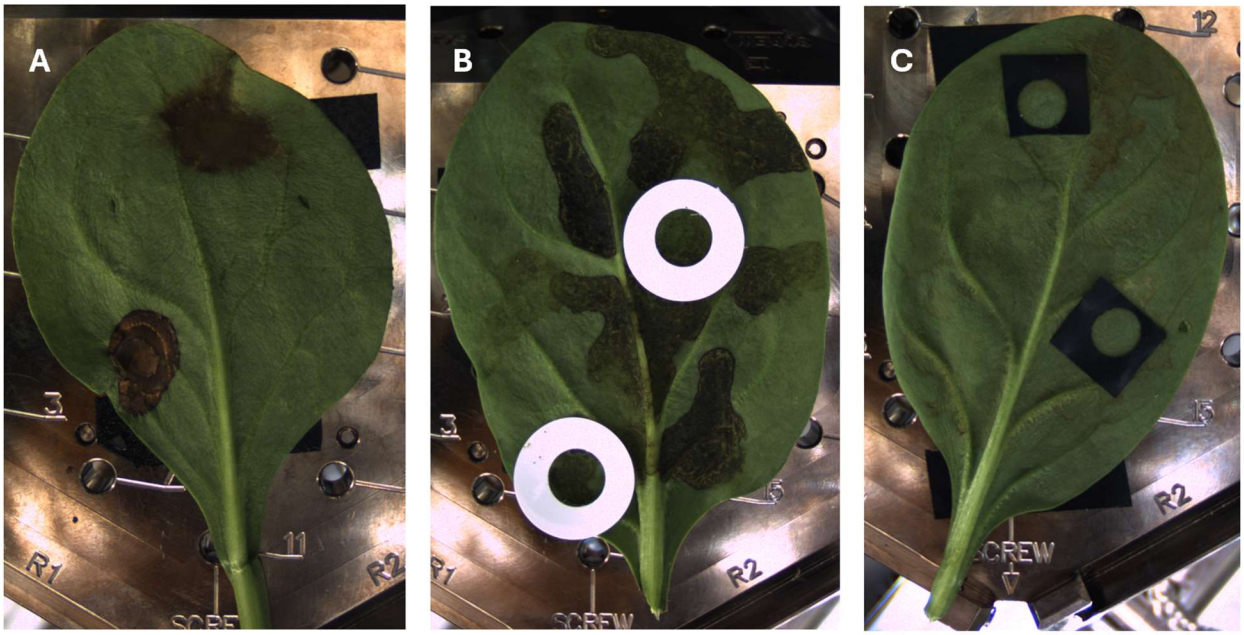

Figure 2. Three methods of applying EPS to fresh leaves: (A) pipetting drops of EPS to create regions, (B) dropping EPS across leaf before selecting regions, and (C) dipping leaf into EPS to create thin layer before selecting regions

Finally, several trials were performed on EPS in the absence of leaves. For these experiments, 3 mL of EPS were pipetted onto 1x3 inch glass slides and allowed to dry. As in the EPS-on-leaf experiments, nanopowder suspension was then pipetted onto the center of each EPS droplet without the need for a tape marker. The final rinsing procedure once again had to be modified. The lack of adhesion between the EPS droplet and slide while wet resulted in frequent instances of complete detachment when submerged vertically. To accommodate this property, the slides were submerged horizontally into a wide bath of rinsing solution. With this orientation not allowing for rinsed and unrinsed regions within the same sample, slides were divided as either fully rinsed or fully unrinsed. The slides were then allowed to dry as normal.

3.2 Imaging Experiments

Once the samples were dried after the final rinse, they were transported in individual Petri dishes to the Samuel Roberts Noble Microscopy Laboratory (SRNML, Laboratory) in Norman, Oklahoma. The number of samples taken to the Laboratory for each session ranged between 4 and 10, with a typical number of 8. Upon the samples' arrival to the SRNML, they were imaged by the Quattro ESEM (environmental scanning electron microscope, "Quattro"). Initial experiments indicated that the samples' exposure to a vacuum was a major challenge to their imaging. At standard vacuum levels, the spinach leaf samples deteriorated substantially within five minutes of Quattro activation, providing an insufficient timespan to image all regions. Figure 3 shows an example of cellular damage sustained from the Quattro's vacuum. Note that once the cells begin to collapse it can be difficult to quantify nanoparticles because the collapsed cells leave networks of hard bright edges that interfere with thresholding analyses.

Later experiments minimized this issue by operating the Quattro in low-vacuum mode (200 Pa), providing around twenty minutes before deterioration became visible. For each leaf placed into the microscope, one backscattered electron image would be taken in the center of each marked region. Several trials included the addition of secondary emission images for modified experiments with image analysis. Blank images, or images taken outside marked regions in deterioration-free areas both with and without a final rise, were also taken as a control and aid in image analysis. Images were primarily taken at 100x magnitude, resulting in a horizontal field width of approximately 2.07 mm. Magnitudes as low as 35x and as high as 12000x were also explored. With the updated process, samples were each in the microscope for an average of ten minutes, well within the bounds of potential deterioration.

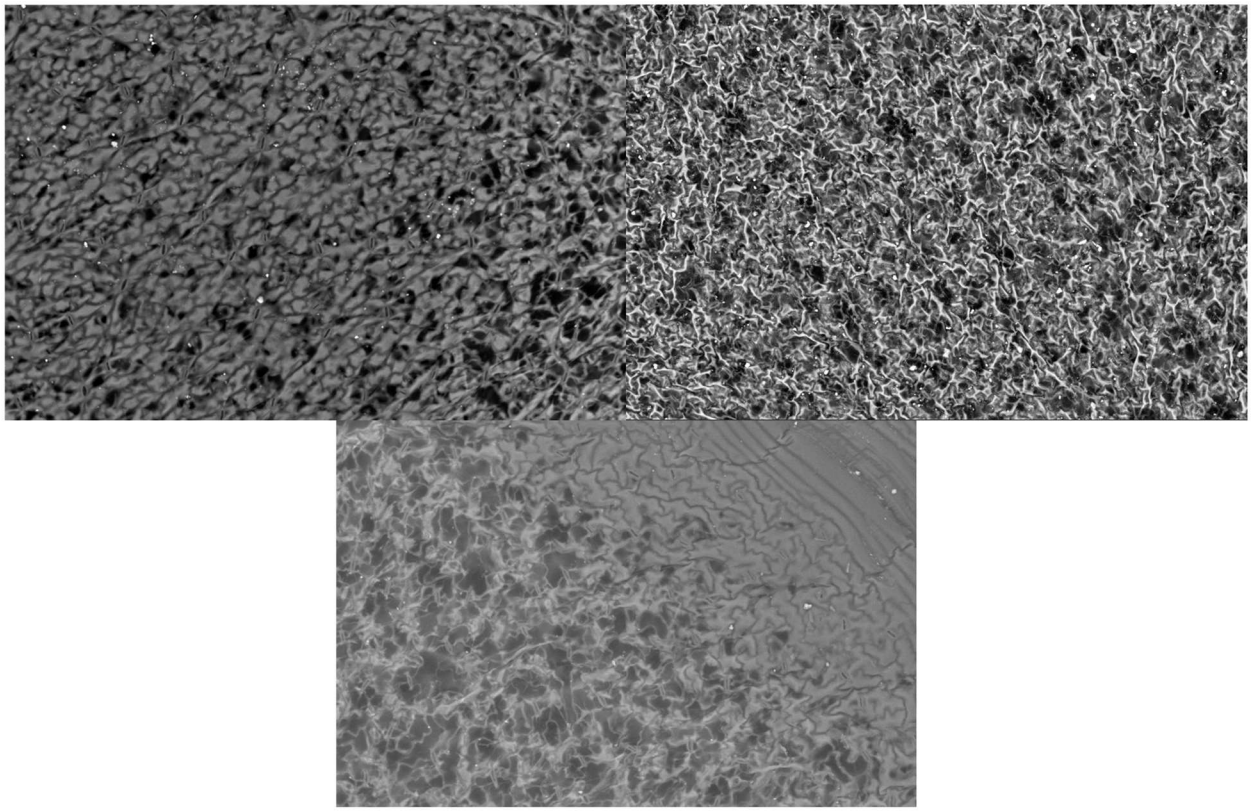

Figure 3. Three *Spinacia oleracea* leaf samples undergoing deterioration from Quattro vacuum. Black zones correspond to collapsed cell structures.

3.3 Alternate Rinsing and Imaging Procedure for EPS Experiments

For selected experiments with EPS, imaging was conducted of the same region both before and after rinsing, to allow direct observation of nanoparticle removal. (Other experiments focused on quantifying average coverage before and after rinsing, but due to the limited stability of spinach leaf surfaces, necessarily focused on different rinsed and unrinsed regions, rather than imaging the same region multiple times.) For this method, EPS-coated slides were placed into the microscope prior to a final rinse, upon which the nanopowder region was identified and a region to be imaged was selected. Once imaged, the distance between the upper borders of the imaged region and the EPS droplet was measured in μm using the Quattro's interface. The slides

were then removed from the microscope and submerged horizontally into a water bath for 60 seconds, after which they were allowed to dry in the SRNML overnight. The following day, the dried slides were returned into the microscope. The region imaged the prior day was first approximated using the measurement collected earlier. The degradation of the EPS droplet border post-final rinse made this match imperfect. To compensate for this effect, the region was matched further using the location of landmarks, such as crystals or large particle clusters. Figure 4 shows a comparison of an EPS slide region before and after a final rinse.

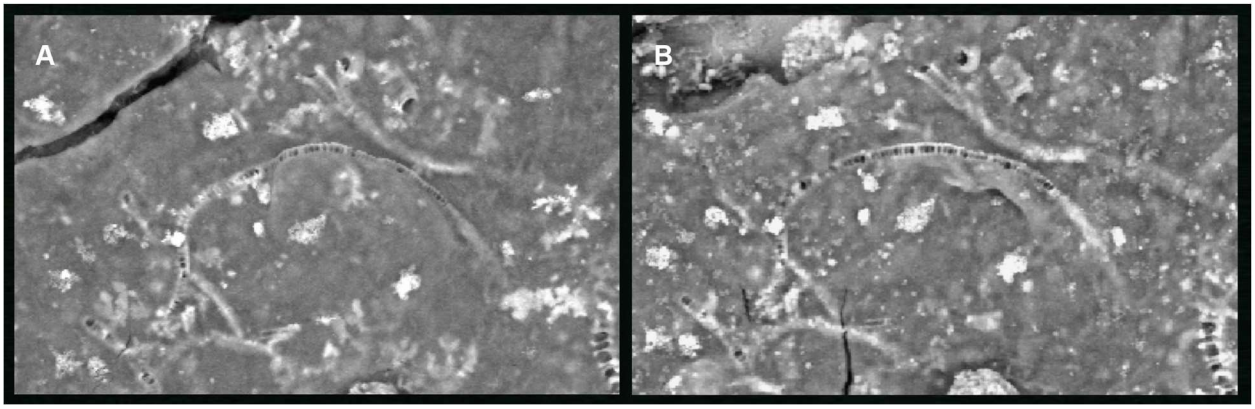

Figure 4. Titanium dioxide on EPS droplet (A) before and (B) after final rinse

3.4 Image Analysis of Backscattered Electron Images

For backscattered electron images, surfaces with higher molecular weight appear brighter. Therefore, quantifying the brightness of pixels within the imaged region can aid in identifying nanoparticles. Initial attempts to quantify nanoparticle coverage relied entirely on existing software ImageJ. While the software was appropriate for image analysis, the brightness threshold for these calculations, scaled from 0-255, needed to be chosen manually. Natural pigmentation variations of the produce rendered a single threshold value insufficient, necessitating the

development of a program that would automatically determine a threshold to be analyzed by ImageJ. The program began by reading a backscattered electron image, which would be transformed in two successive ways: firstly, into a grayscale image format, to improve processing time, and secondly, into an array of each pixel's brightness level. The function $f(x)$ was then defined as giving the number of values in the array greater than x, effectively numbering the pixels brighter than a certain value. One such function is shown in Figure 5. Note that the figure shows a dramatic decrease around levels 70 to 150 – this is the approximate range of spinach cell brightness, constituting a majority of the input image.

The threshold T was then defined as:

$$T = g^{-1}(S)$$

where

$$S = \max_{x \in [n]} g(x) + 0.01(\min g + \max g)$$

$$g = g(x) = f'(x)$$

and

$$[n] = \{\lfloor \text{argmin} g(x) \rfloor, \cdots, 255\}$$

Determining the most appropriate value for T required calculating derivatives of the original function. The first derivative of $f(x)$, denoted $g(x)$, shown in Figure 5, provided a clearer view as to the components of the image: the plateaued left third, from a brightness

intensity range of approximately 0 to 70, representing the black cell borders; the middle depression, from 70 to 150, representing the spinach cells; and the plateaued right third, from 150 to 255, representing the bright nanoparticles on the spinach surface. To select a baseline for the threshold, the point on the right third of the function at which the rate of decrease was lowest was chosen, denoted $\max_{x\in[n]} g(x)$. With $f(x)$ being a reverse-cumulative distribution, $g(x)$ would always be negative, and the maximum of this function would be the point with the least absolute value. The bounds $[n]$ were specified in the event that $\max(g)$ was located in the left third of $g(x)$, a frequent occurrence in image testing. To eliminate the left third, the brightness level of the nadir of the depression, $\lfloor \text{argmin} g(x) \rfloor$, was selected as the left bound, with the maximum x value, 255, was selected as the right bound. This baseline alone was insufficient in identifying all nanoparticles. A larger range was selected by reducing the threshold slope by a magnitude of 1% of the total range of $g(x)$. This new threshold slope provided a satisfactory threshold between nanoparticles and non-nanoparticle pixels.

With the data from Figure 5, the calculation was performed as follows:

$$\min g = -26972.5$$

$$\max g = -647.5$$

$$\lfloor \text{argmin} g(x) \rfloor = 104$$

$$\max_{x\in[n]} g(x) = -647.5$$

$$S = -910.75$$

$$T = 221$$

Figure 5.A shows the corresponding $f(x)$ for a single image of zinc oxide at 200 mg/L concentration. This figure was then transformed via derivation into Figure 5.B, which has had several defining features overlaid. S, the threshold slope, and T, the brightness intensity at the threshold slope, are marked on the figure. In addition, $[\text{argmin} g(x)]$, the lower bound of the range at which $\max g(x)$ was identified, is shown as the dashed line. In this case, the maximum value of g across all values of x was the same as across the set $[n]$. However, in certain cases, lack of intensely dark regions on the image can create a shallow initial decrease, therefore causing $\max g$ to be outside $[n]$. In such cases, the specification of the set is necessary.

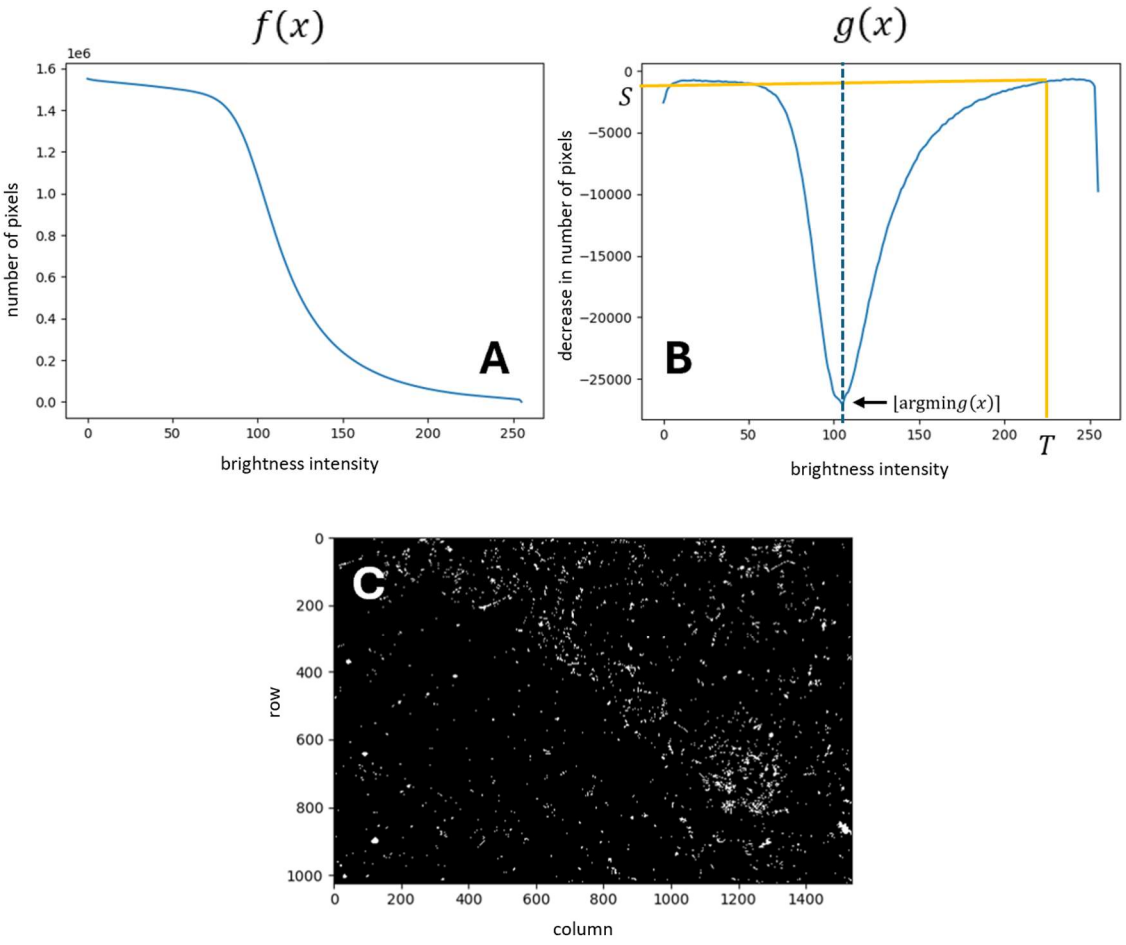

Figure 5. Three outputs from the developed program: (A) $f(x)$, plotting the number of pixels in the inputted image above a certain brightness level; (B) $g(x)$, plotting the first derivative of $f(x)$; (C) the inputted image transformed to display only pixels above the calculated threshold

With the threshold established, the image was put back together with the brightness level $b(x)$ of each pixel updated as follows:

$$b(x) = \begin{cases} 0, & x < T \\ 255, & x \geq T \end{cases}$$

In effect, this creates a binary image in which all pixels deemed to belong to nanoparticles are colored white, and all other pixels are colored black. An example of one such thresholded output can be seen in Figure 6.C, alongside an image inputted to the thresholding program (Figure 6.A) and an image manually thresholded using existing software (Figure 6.B). In addition to returning the binary image, the program also gave the number of pixels with $x \geq T$, a quantification of nanoparticle coverage in the imaged region. Following this manipulation, the image could be analyzed by ImageJ to explore more statistics such as the number of nanoparticle "clusters" (regions of connected pixels) and average cluster size.

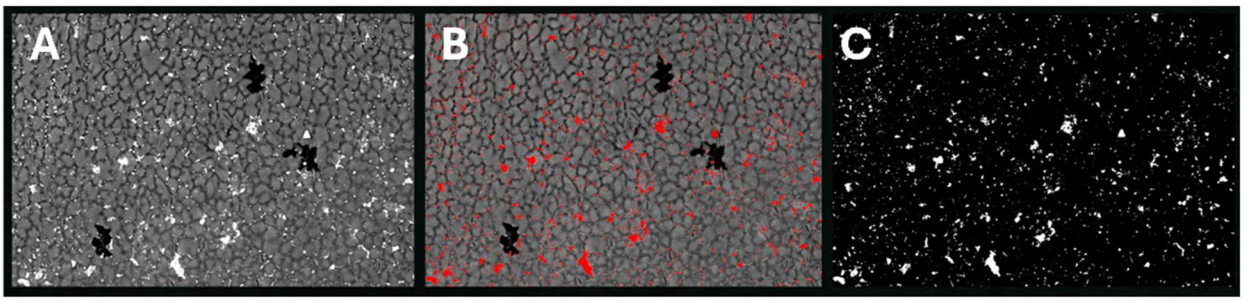

Figure 6. Three forms of an image from the Quattro: (A) the image in its original form, cropped to remove legend, (B) the image after only an ImageJ manual thresholding, and (C) the image after being thresholded by the developed program

The final program was largely effective at identifying pixels deemed to be nanoparticles, particularly for images of nanoparticles on fresh spinach. Experiments with EPS were more

challenging, due to the occurrence of crystals and tubular structures which were difficult to distinguish from nanoparticles on brightness alone. The crystals were analyzed using the Quattro's spectrometry capabilities. Elements found in such crystals include calcium, nickel, potassium, iron, phosphorus, and magnesium. While the tubular structures were theorized to be of an organic nature, they were never identified. Another complication with EPS was its tendency to fracture when drying, leaving fissures within the imaged regions. Such gaps would cause the microscope to directly image the glass slide underneath the sample. The slide's refractive properties would then create a glare of a high brightness level, which would be picked up as nanoparticles. These complications are shown in Figure 7. In addition to EPS, a few experiments with fresh leaves encountered difficulties with the program. In some cases, the natural variation in leaf pigmentation led to a particularly bright sample surface, whose cell walls were at points indistinguishable from nanoparticles in brightness level alone. For these reasons, quantitative analysis of nanoparticle attachment to samples containing EPS was not possible in all but a few cases where very low quantities of EPS were applied.

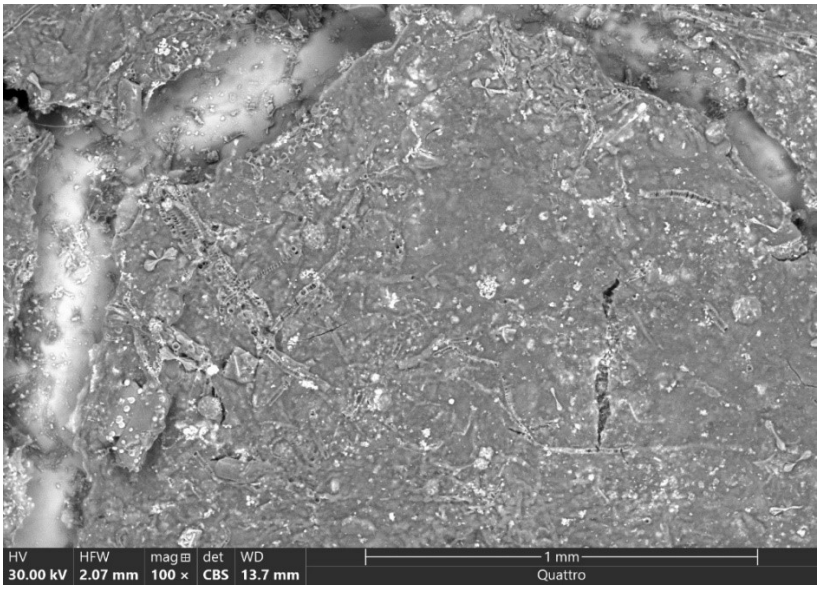

Figure 7. Complications arising from EPS on a glass slide. Glare from the slide occurs across the left side, and tubular structures can be seen throughout

4. RESULTS AND DISCUSSION

A total of 139 images were analyzed by the thresholding program and image analysis software. The samples each had several variables that potentially impact nanoparticle detachment, such as the type of nanoparticle, pH of rinsing solution, concentration of nanopowder suspension, and presence of EPS. T-tests were performed on all data sets to check for statistical significance. Results from t-tests are omitted when lack of significance is trivial.

4.1 Concentration Results

Figures 8 and 9 show image analysis results from a 200 mg/L nanopowder suspension application with varying nanoparticle conditions. The average number of thresholded pixels, or pixels deemed to be nanoparticles, are shown for the two nanoparticles studied for both rinsed and unrinsed samples. Error bars of one standard deviation are also shown. With zinc oxide applied to fresh, dry leaves, removal of nanoparticles can be observed after rinsing. The samples have 43.3% fewer thresholded pixels and 16.4% fewer clusters than the unrinsed samples. The discrepancy between these two values indicates that larger particle clusters are removed at a higher rate than those smaller. The average cluster size decreased 36.2%, from 12.9 pixels to 8.3. This decrease in particle count was present, but less pronounced, for samples containing titanium dioxide.

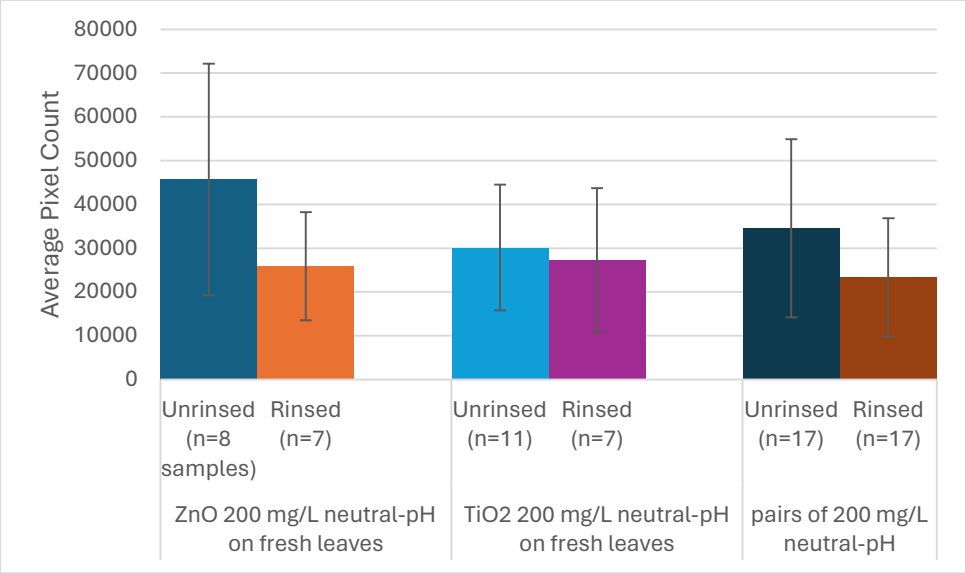

Figure 8. Average pixel count for 200 mg/L samples without and with rinse. Each pair of bars corresponds to one set of conditions.

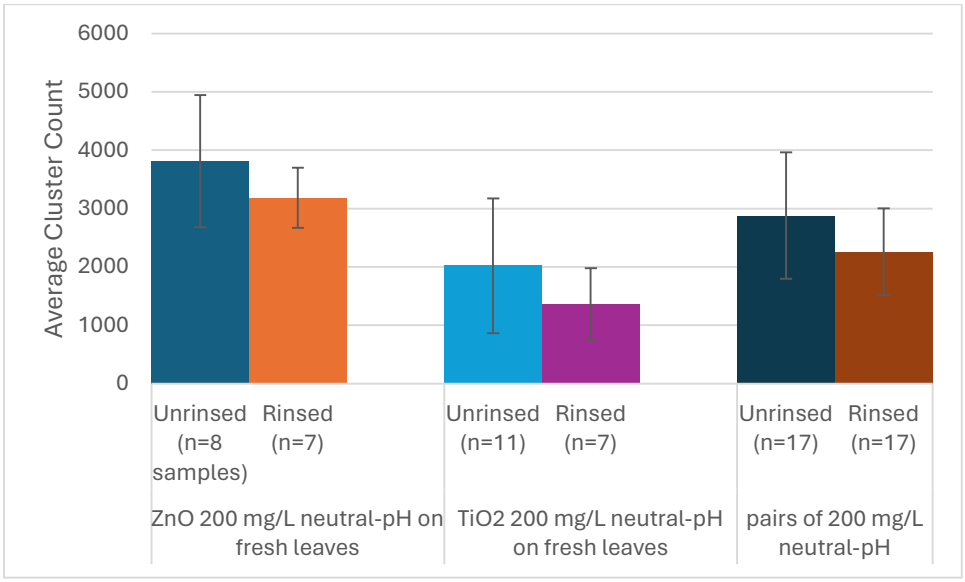

Figure 9. Average cluster count for 200 mg/L samples without and with rinse

An unpaired t-test was performed on the data to check for statistical significance in a decrease in zinc oxide coverage at 200 mg/L. The first test involved two sets: one containing the pixel count from all 200 mg/L unrinsed regions on a fresh, dry leaf, and the other containing its rinsed counterpart. As the unrinsed regions' standard deviation was over twice that of the rinsed regions, the variances of the two sets were not assumed to be equal. The p-value from the resulting two-tailed t-test was .087, which is not enough to state statistical significance at a confidence level of 95%. In addition, a paired t-test was performed on the average particle count with and without rinse from each leaf. This procedure eliminates the issue of high variance of pigmentation between separate leaves. The p-value from this test was 0.111, again not enough to claim statistical significance. However, the number of 200 mg/L zinc oxide pairs on fresh leaves rinsed at neutral pH was at a level considerably low as to inhibit significance (n=5 pairs). Increasing the set of pairs to all neutral-pH samples with 200 mg/L nanopowder suspension, regardless of leaf freshness, a paired t-test results in a p-value of .042 (n=16 pairs). With an alpha level of 0.05, it can be said that for samples coated in 200 mg/L nanopowder, a 60-second rinse in a neutral-pH solution was significantly effective in removing nanoparticles. The results of these t-tests are shown in the Appendix.

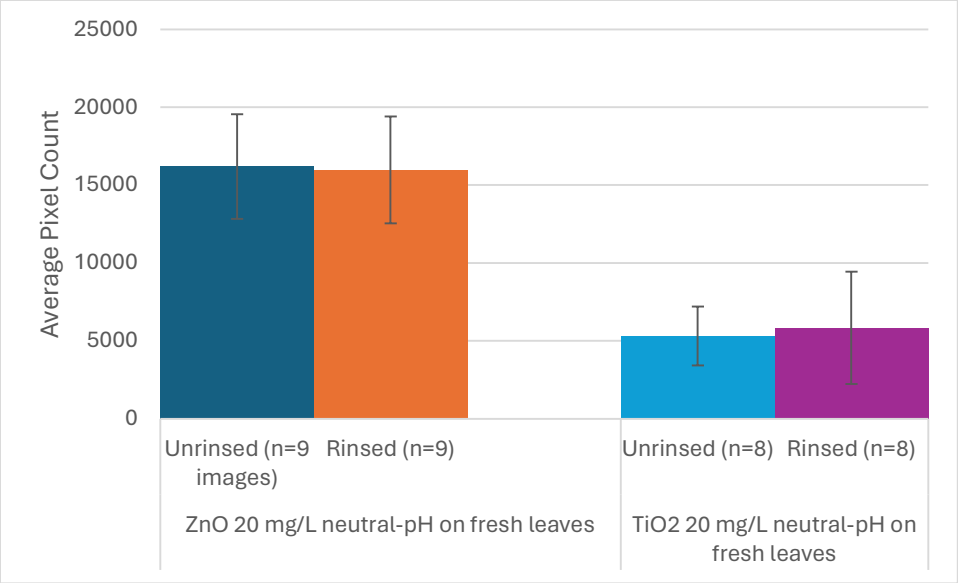

Figure 10. Average pixel count for 20 mg/L samples without and with rinse

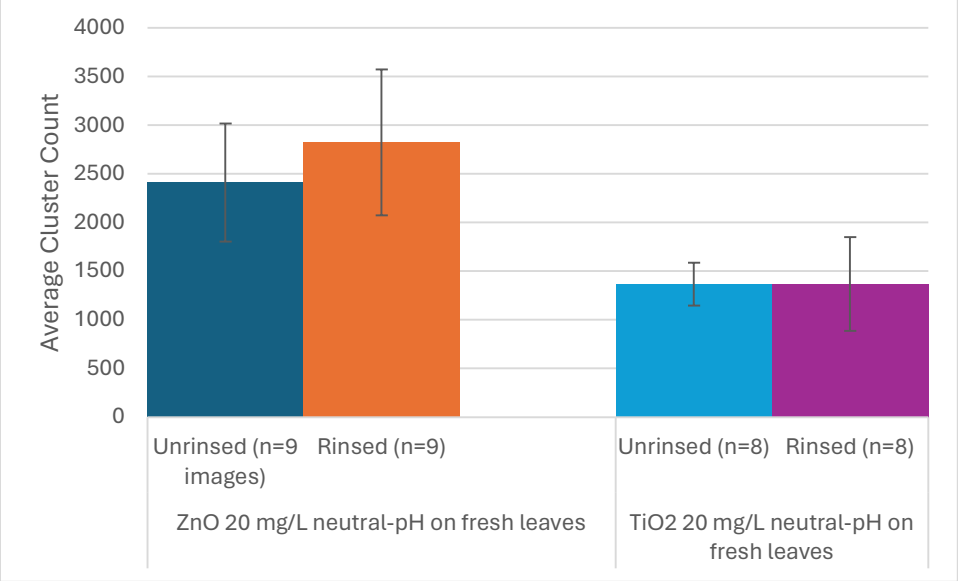

Figure 11. Average cluster count for 20 mg/L samples without and with rinse

Figures 10 and 11 show image analysis results from samples at 20 mg/L concentration. At 20 mg/L, no statistically significant decrease in nanoparticle coverage or cluster size can be observed. Rinsed samples of both zinc oxide and titanium dioxide on fresh leaves show less than 10% difference in pixel count compared to unrinsed samples. A paired t-test of cluster counts at this concentration resulted in a p-value of .187 (n=17 pairs), indicating that there is not a statistically significant increase in cluster counts after rinse for 20 mg/L samples. While the total coverage across the entire drop should be consistent for each region, the imaged region is only a fraction of the drop. Therefore, an imaged region could have a heightened initial nanoparticle coverage such that not enough is removed during rinsing to fall behind the unrinsed region on the same leaf.

4.2 Surface Results

Figures 12 and 13 show image analysis results from samples imaged on fresh and EPS-added surfaces. Quantification of images with EPS proved difficult due to their ease of detachment and proclivity to have non-nanoparticle substances on their surfaces. For these reasons, data is limited for EPS analysis. Still, the results show that the addition of EPS had an insignificant effect on nanoparticle detachment at 200 mg/L compared with fresh leaves. With pH and nanoparticle equal for all samples, rinsing resulted in an average decrease of 9.6% for fresh leaves and 12.2% for samples with EPS.

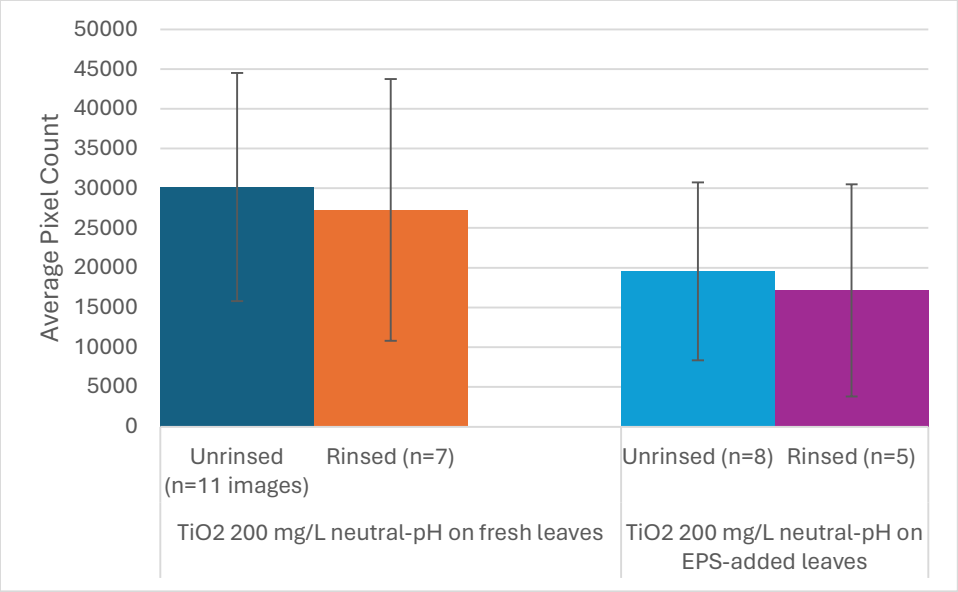

Figure 12. Average pixel count for 200 mg/L neutral-pH titanium dioxide samples without and with rinse

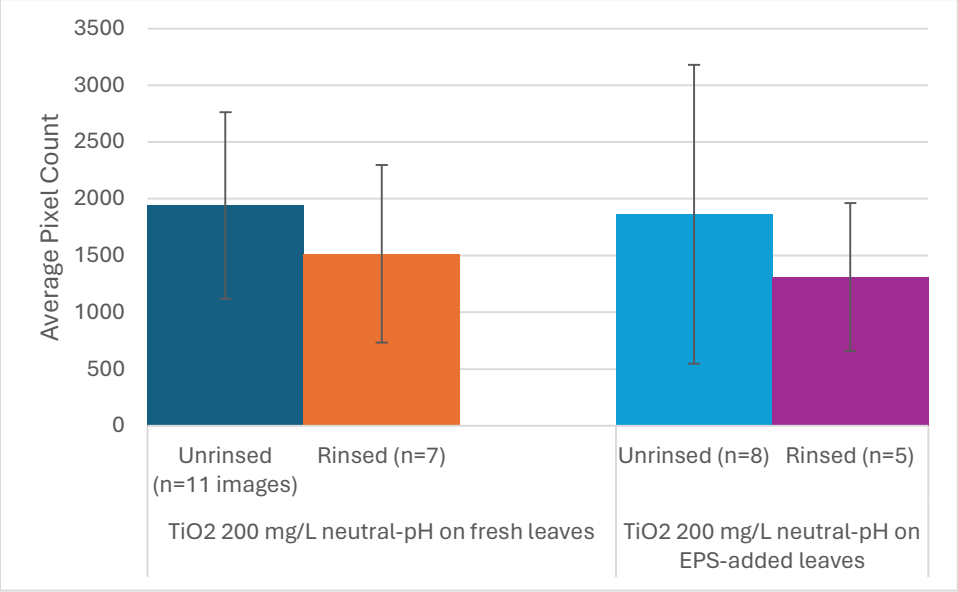

Figure 13. Average cluster count for 200 mg/L neutral-pH titanium dioxide samples without and with rinse

Average cluster count also remained relatively consistent from fresh leaves to leaves with EPS. This result matched with the noticeable lower initial and final particle counts from leaves with EPS indicate that initial attachment favorability was lowered by the substances' presence.

One phenomenon observed during trials involving EPS was its partial removal after rinsing. While a vertical bath resulted frequently in complete detachment of the sample, horizontal baths also saw some EPS detachment. Figure 14 shows the deterioration of the sample's outer border. In addition to complicating the relocation of the imaged region, this also opened the possibility of its upper layer experiencing partial detachment. In this event, nanoparticles attached to the EPS would not have to detach to be removed from the sample.

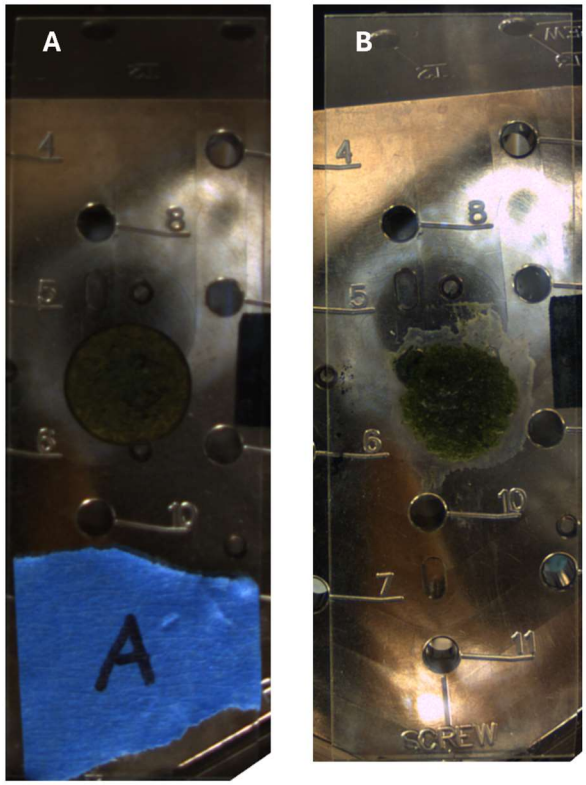

Figure 14. Removal of EPS after final rinse. Tape was removed from the slide prior to rinse.

4.3 pH and Zeta Potential Analysis

Zeta potential is a measurement of electric charge used to calculate the attractive force between two surfaces. Charged particles exposed to liquids often have two surrounding layers: the inner layer, where ions are tightly bound to the particle, and the outer layer, where ions are more loosely bound. The electric potential within the outer layer is the zeta potential (Kaszuba et al., 2010). At a higher positive zeta potential, a particle will be more inclined to attach to a negatively charged surface. Therefore, measuring this property for the particles tested can provide insight to their attachment results.

Samples of zinc oxide suspension were created at varying pH levels. Each suspension consisted of 3 mL of the 200 mg/L neutral-pH zinc oxide suspension used for surface application. 27 mL of pH adjustments were then added, ranging from entirely 0.01 M hydrochloric acid to an acid solution progressively diluted with DI water, to entirely DI water, to an alkaline solution diluted with DI water, and finally entirely 0.01 M sodium hydroxide. A total of 11 samples were created. The samples were then individually pipetted into vials and placed into a zeta potential analyzer, whose results are plotted in Figure 15.

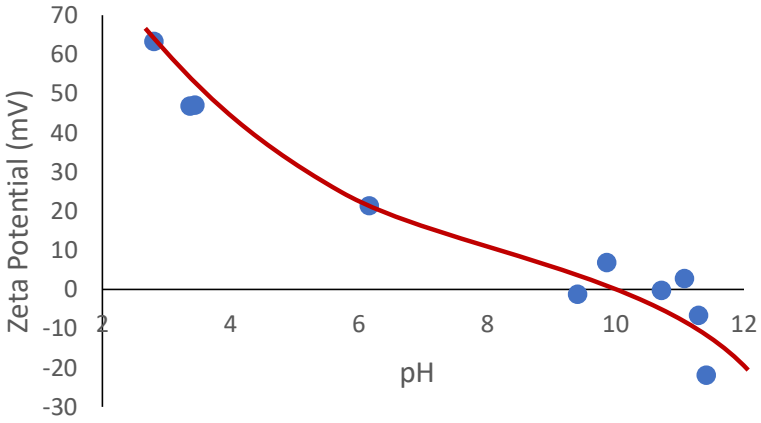

Figure 15. Zeta potential of zinc oxide vs. pH

The zeta potential shows a relatively stable decrease from a lower pH to a higher pH. This property crosses a threshold between pH 9 and 10, going from a positive charge to negative. This point is referred to as the point of zero charge (PZC). This result is like those reported in literature, with PZC values for zinc oxide ranging from 8.4 to 9.0 (Khataee et al., 2016; Yashni et al., 2020; Zyoud et al., 2023). In theory, as zinc oxide approaches its PZC from a lower pH, its ability to attach to negatively charged surfaces is diminished. This effect is also true for titanium dioxide, whose 20 mg/L samples on fresh leaves were the primary focus of imaging experiments in varying pH. The PZC of titanium dioxide is reported at around 5.8 (Kosmulski, 2002). However, the titanium dioxide samples rinsed in high-pH solution did not show significantly more detachment than those rinsed in neutral-pH solution. As seen in Figures 16 and 17, at a concentration of 20 mg/L, titanium dioxide leaves rinsed in a high-pH solution (8.35) showed a 7.1% increase in particle coverage, a similar statistic as the 9.8% increase in a neutral-pH solution (6.02). The results for cluster count are also nearly identical. The high-pH leaves showed a 1.6% decrease in average cluster count, while the neutral-pH leaves showed a 0.1% increase. The results indicate there could be other interactions responsible for the discrepancies seen in particle removal.

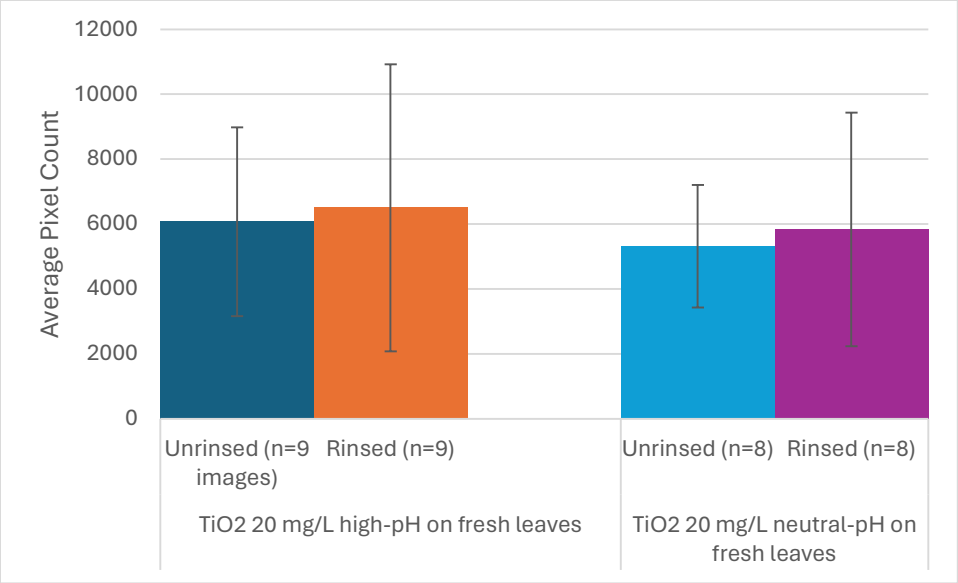

Figure 16. Average pixel count for selected 20 mg/L titanium dioxide samples without and with rinse

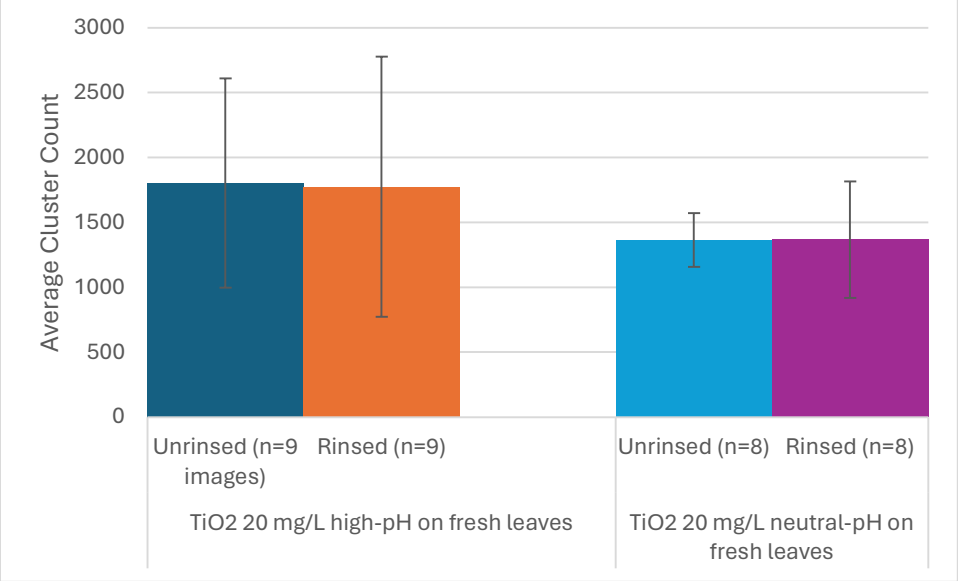

Figure 17. Average cluster count for selected 20 mg/L titanium dioxide samples without and with rinse

4.4 Summary

Figure 18 shows the percent decrease in average thresholded pixel count per image for rinsed images as opposed to unrinsed images. Statistically significant removal was observed after rinsing in samples with a 200 mg/L nanoparticle suspension application across various conditions. This variable was the only one to result in a statistically significant decrease in pixel count. Changes in surface freshness, as well as pH, did not result in a statistically significant change in the percentage of nanoparticle detachment. Zinc oxide's high PZC compared to titanium dioxide means attachment could be less favored in samples with titanium dioxide, whose neutral-pH solutions are slightly above its PZC, resulting in a slightly negative charge interacting with the negative surface charge of the produce. However, for both 200 mg/L and 20 mg/L concentrations, more removal was observed for zinc oxide samples than titanium dioxide. One potential phenomenon that could be overriding the particle-spinach interactions is particle-particle interactions. At particularly high magnitudes of zeta potential, particle clusters could be repelling other clusters and encouraging detachment regardless of particle-produce properties. These high magnitudes are exhibited at pHs far from a particle's PZC. With this in mind, titanium dioxide at neutral pH, close to its PZC of 5.8, should show less detachment than zinc oxide at neutral pH or titanium dioxide at high pH. Indeed, at 20 mg/L, titanium dioxide at neutral pH showed the least detachment, followed by titanium dioxide at high pH and finally zinc oxide at neutral pH. The order of the remaining two also falls in line with this theory, as the high-pH solution (pH=8.35) is slightly closer to titanium dioxide's PZC than the neutral-pH solution (pH=6.02) is to zinc oxide's PZC (around 9). At higher concentrations, smaller boundaries between particle clusters would magnify this effect. This could be an explanation for the higher detachment rates at high concentration. At 200 mg/L, zinc oxide at neutral pH once

again shows more detachment than titanium dioxide at neutral pH, and this difference is exacerbated. The differences in percent decrease between the two nanoparticles are 34% at higher 200 mg/L and 11% at 20 mg/L. These results indicate that interactions between particles could be a more defining characteristic in particle detachment than interactions between particles and produce surfaces.

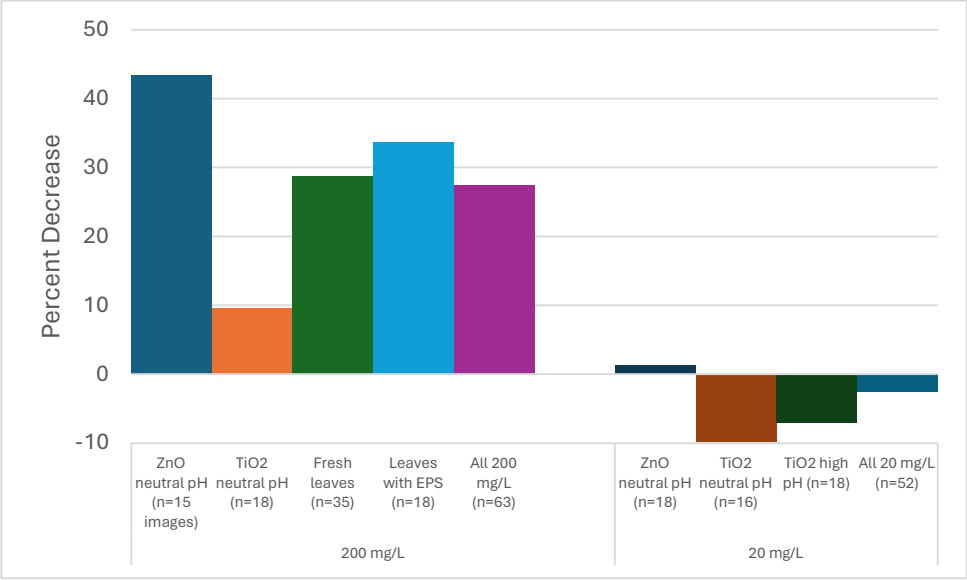

Figure 18. Percent decrease in pixel count after final rinse for various conditions at two concentrations

CONCLUSION

The ability for nanoparticles to aid the agricultural world, as well as potentially harm consumers, depends on their tendency to attach to organic surfaces. The objective of this work was the development of a rinsing procedure to allow for a comparison of samples across various pH values, nanoparticle concentrations, and freshness with and without submergence in a water-based solution. In tandem with this procedure, an image analysis program was created to automatically threshold nanoparticles from non-nanoparticles. Finally, the relationship between nanoparticle coverage, in total magnitude as well as clustering tendencies, was explored across several variables.

The developed image analysis program was successful in identifying nanoparticles on produce surfaces. However, the rinsing procedure was largely ineffective at removing nanoparticles across changes in pH, surface type, and nanoparticle type. The only statistically significant removal occurred in samples with 200 mg/L concentration, as opposed to 20 mg/L. This effect could be due to electrostatic interactions between particles on the produce surface, which also could provide insight as to higher removal levels for zinc oxide than titanium dioxide. It was expected that pH variations and an introduction to EPS would see a significant change in nanoparticle removal. However, the changes seen were not statistically significant. For the former, additional research into the magnitude of the zeta potential of attached nanoparticles in relation to other electrostatic forces would be beneficial. For the latter, continued work in developing a method in which samples are rinsed without high removal of EPS could provide more insight into its true effect on nanoparticle detachment. In addition to the recommendations above, further research into established methods of pH and nanoparticle variation could garner more significance in results.

REFERENCES

Adair, J. H., Suvaci, E., & Sindel, J. (2001). Surface and Colloid Chemistry. In K. H. J. Buschow, R. W. Cahn, M. C. Flemings, B. Ilschner, E. J. Kramer, S. Mahajan, & P. Veyssière (Eds.), *Encyclopedia of Materials: Science and Technology* (pp. 1-10). Elsevier. https://doi.org/https://doi.org/10.1016/B0-08-043152-6/01622-3

Adil, M., Bashir, S., Bashir, S., Aslam, Z., Ahmad, N., Younas, T., Asghar, R. M. A., Alkahtani, J., Dwiningsih, Y., & Elshikh, M. S. (2022). Zinc oxide nanoparticles improved chlorophyll contents, physical parameters, and wheat yield under salt stress [Original Research]. *Frontiers in Plant Science*, *13*. https://doi.org/10.3389/fpls.2022.932861

Aschner, M. (2009). Chapter 8 - Nanoparticles: Transport across the olfactory epithelium and application to the assessment of brain function in health and disease. In H. S. Sharma (Ed.), *Progress in Brain Research* (Vol. 180, pp. 141-152). Elsevier. https://doi.org/https://doi.org/10.1016/S0079-6123(08)80008-8

Dai, Q., Wilhelm, S., Ding, D., Syed, A. M., Sindhwani, S., Zhang, Y., Chen, Y. Y., MacMillan, P., & Chan, W. C. W. (2018). Quantifying the Ligand-Coated Nanoparticle Delivery to Cancer Cells in Solid Tumors. *ACS Nano*, *12*(8), 8423-8435. https://doi.org/10.1021/acsnano.8b03900

Dekkers, S., Krystek, P., Peters, R. J., Lankveld, D. P., Bokkers, B. G., van Hoeven-Arentzen, P. H., Bouwmeester, H., & Oomen, A. G. (2011). Presence and risks of nanosilica in food products. *Nanotoxicology*, *5*(3), 393-405.

Derjaguin, B., & Landau, L. (1993). Theory of the stability of strongly charged lyophobic sols and of the adhesion of strongly charged particles in solutions of electrolytes. *Progress in*

Surface Science, *43*(1), 30-59. https://doi.org/https://doi.org/10.1016/0079-6816(93)90013-L

Gohari, G., Mohammadi, A., Akbari, A., Panahirad, S., Dadpour, M. R., Fotopoulos, V., & Kimura, S. (2020). Titanium dioxide nanoparticles (TiO2 NPs) promote growth and ameliorate salinity stress effects on essential oil profile and biochemical attributes of Dracocephalum moldavica. *Scientific Reports*, *10*(1), 912. https://doi.org/10.1038/s41598-020-57794-1

Hou, J., Wang, L., Wang, C., Zhang, S., Liu, H., Li, S., & Wang, X. (2019). Toxicity and mechanisms of action of titanium dioxide nanoparticles in living organisms. *Journal of Environmental Sciences*, *75*, 40-53. https://doi.org/https://doi.org/10.1016/j.jes.2018.06.010

Hunter, R. J. (1989). "Colloidal systems and interfaces", By S. Ross and I. D. Morrison. 1st Ed. (1988) pp. xviii + 422. John Wiley and Son, New York. Price $us 49.95. *The Canadian Journal of Chemical Engineering*, *67*(1), 175-176. https://doi.org/https://doi.org/10.1002/cjce.5450670128

Ilett, M., Wills, J., Rees, P., Sharma, S., Micklethwaite, S., Brown, A., Brydson, R., & Hondow, N. (2020). Application of automated electron microscopy imaging and machine learning to characterise and quantify nanoparticle dispersion in aqueous media. *Journal of Microscopy*, *279*(3), 177-184. https://doi.org/https://doi.org/10.1111/jmi.12853

Ji, Z., Ismail, M. N., Callahan, D. M., Pandowo, E., Cai, Z., Goodrich, T. L., Ziemer, K. S., Warzywoda, J., & Sacco, A. (2011). The role of silver nanoparticles on silver modified titanosilicate ETS-10 in visible light photocatalysis. *Applied Catalysis B: Environmental*, *102*(1), 323-333. https://doi.org/https://doi.org/10.1016/j.apcatb.2010.12.021

Kannan, K., & Vimalkumar, K. (2021). A Review of Human Exposure to Microplastics and Insights Into Microplastics as Obesogens [Review]. *Frontiers in Endocrinology*, *12*. https://doi.org/10.3389/fendo.2021.724989

Kaszuba, M., Corbett, J., Watson, F. M., & Jones, A. (2010). High-concentration zeta potential measurements using light-scattering techniques. *Philos Trans A Math Phys Eng Sci*, *368*(1927), 4439-4451. https://doi.org/10.1098/rsta.2010.0175

Khataee, A., Kıranşan, M., Karaca, S., & Arefi-Oskoui, S. (2016). Preparation and characterization of ZnO/MMT nanocomposite for photocatalytic ozonation of a disperse dye. *TURKISH JOURNAL OF CHEMISTRY*, *40*, 546-564. https://doi.org/10.3906/kim-1507-77

Kosmulski, M. (2002). The significance of the difference in the point of zero charge between rutile and anatase. *Adv Colloid Interface Sci*, *99*(3), 255-264. https://doi.org/10.1016/s0001-8686(02)00080-5

Krishna, V., Pumprueg, S., Lee, S.-H., Zhao, J., Sigmund, W., Koopman, B., & Moudgil, B. (2005). Photocatalytic disinfection with titanium dioxide coated multi-wall carbon nanotubes. *Process Safety and Environmental Protection*, *83*(4), 393-397.

Lei, Z., Mingyu, S., Xiao, W., Chao, L., Chunxiang, Q., Liang, C., Hao, H., Xiaoqing, L., & Fashui, H. (2008). Antioxidant Stress is Promoted by Nano-anatase in Spinach Chloroplasts Under UV-B Radiation. *Biological Trace Element Research*, *121*(1), 69-79. https://doi.org/10.1007/s12011-007-8028-0

Liu, J., Fan, Y., Sun, Y., Wang, Z., Zhao, D., Li, T., Dong, B., & Tang, C. Y. (2021). Modelling the critical roles of zeta potential and contact angle on colloidal fouling with a coupled

XDLVO - collision attachment approach. *Journal of Membrane Science*, *623*, 119048. https://doi.org/https://doi.org/10.1016/j.memsci.2021.119048

Lu, K., Zhan, D., Fang, Y., Li, L., Chen, G., Chen, S., & Wang, L. (2022). Microplastics, potential threat to patients with lung diseases. *Front Toxicol*, *4*, 958414. https://doi.org/10.3389/ftox.2022.958414

Medina, C., Santos-Martinez, M. J., Radomski, A., Corrigan, O. I., & Radomski, M. W. (2007). Nanoparticles: pharmacological and toxicological significance. *Br J Pharmacol*, *150*(5), 552-558. https://doi.org/10.1038/sj.bjp.0707130

Mi, K., Yuan, X., Wang, Q., Dun, C., Wang, R., Yang, S., Yang, Y., Zhang, H., & Zhang, H. (2023). Zinc oxide nanoparticles enhanced rice yield, quality, and zinc content of edible grain fraction synergistically. *Front Plant Sci*, *14*, 1196201. https://doi.org/10.3389/fpls.2023.1196201

Mittal, D., Kaur, G., Singh, P., Yadav, K., & Ali, S. A. (2020). Nanoparticle-Based Sustainable Agriculture and Food Science: Recent Advances and Future Outlook [Review]. *Frontiers in Nanotechnology*, *2*. https://doi.org/10.3389/fnano.2020.579954

Mortvedt, J. J., & Gilkes, R. J. (1993). Zinc fertilisers. In *Zinc in Soils and Plants* (pp. 33-44). Dordrecht: Kluwer Academic Publishers.

Powers, K. W., Brown, S. C., Krishna, V. B., Wasdo, S. C., Moudgil, B. M., & Roberts, S. M. (2006). Research strategies for safety evaluation of nanomaterials. Part VI. Characterization of nanoscale particles for toxicological evaluation. *Toxicol Sci*, *90*(2), 296-303. https://doi.org/10.1093/toxsci/kfj099

Roohinejad, S., & Greiner, R. (2016). Nanoscience: Relevance for Agriculture and the Food Sector. In. https://doi.org/10.1002/9783527697724.ch20

Shemawar, Mahmood, A., Hussain, S., Mahmood, F., Iqbal, M., Shahid, M., Ibrahim, M., Ali, M. A., & Shahzad, T. (2021). Toxicity of biogenic zinc oxide nanoparticles to soil organic matter cycling and their interaction with rice-straw derived biochar. *Scientific Reports*, *11*(1), 8429. https://doi.org/10.1038/s41598-021-88016-x

Sheth, V., Chen, X., Mettenbrink, E. M., Yang, W., Jones, M. A., M'Saad, O., Thomas, A. G., Newport, R. S., Francek, E., Wang, L., Frickenstein, A. N., Donahue, N. D., Holden, A., Mjema, N. F., Green, D. E., DeAngelis, P. L., Bewersdorf, J., & Wilhelm, S. (2023). Quantifying Intracellular Nanoparticle Distributions with Three-Dimensional Super-Resolution Microscopy. *ACS Nano*, *17*(9), 8376-8392. https://doi.org/10.1021/acsnano.2c12808

Shivay, Y., Kumar, D., Prasad, R., & Ahlawat, I. (2008). Relative yield and zinc uptake by rice from zinc sulphate and zinc oxide coatings onto urea. *Nutrient Cycling in Agroecosystems*, *80*, 181-188. https://doi.org/10.1007/s10705-007-9131-5

Shvedchenko, D. O., & Suvorova, E. I. (2017). Combination of thresholding and fitting methods for measuring nanoparticle sizes and size distributions in (S)TEM. *Microscopy Research and Technique*, *80*(10), 1113-1122. https://doi.org/https://doi.org/10.1002/jemt.22908

Takkar, P. N., & Walker, C. D. (1993). The distribution and correction of zinc deficiency. In *Zinc in Soils and Plants* (pp. 151-166). Dordrecht: Kluwer Academic Publishers.

Tulchinsky, T. H. (2010). Micronutrient Deficiency Conditions: Global Health Issues. *Public Health Reviews*, *32*(1), 243-255. https://doi.org/10.1007/BF03391600

van Oss, C. J. (1993). Acid—base interfacial interactions in aqueous media. *Colloids and Surfaces A: Physicochemical and Engineering Aspects*, *78*, 1-49. https://doi.org/https://doi.org/10.1016/0927-7757(93)80308-2

Verwey, E. J. W. (1947). Theory of the Stability of Lyophobic Colloids. *The Journal of Physical and Colloid Chemistry*, *51*(3), 631-636. https://doi.org/10.1021/j150453a001

Vianello, A., Jensen, R. L., Liu, L., & Vollertsen, J. (2019). Simulating human exposure to indoor airborne microplastics using a Breathing Thermal Manikin. *Scientific Reports*, *9*(1), 8670. https://doi.org/10.1038/s41598-019-45054-w

Wang, Z. (2016). A New Approach for Segmentation and Quantification of Cells or Nanoparticles. *IEEE Transactions on Industrial Informatics*, *12*(3), 962-971. https://doi.org/10.1109/TII.2016.2542043

Yashni, G., Al-Gheethi, A., Mohamed, R., & Al-Sahari, M. (2020). Reusability performance of green zinc oxide nanoparticles for photocatalysis of bathroom greywater. *Water Practice and Technology*, *16*(2), 364-376. https://doi.org/10.2166/wpt.2020.118

Zyoud, A., Zyoud, A. H., Zyoud, S. H., Nassar, H., Zyoud, S. H., Qamhieh, N., Hajamohideen, A., & Hilal, H. S. (2023). Photocatalytic degradation of aqueous methylene blue using ca-alginate supported ZnO nanoparticles: point of zero charge role in adsorption and photodegradation. *Environ Sci Pollut Res Int*, *30*(26), 68435-68449. https://doi.org/10.1007/s11356-023-27318-1

APPENDIX

Table 1. Result of t-test for pixel count: paired samples of zinc oxide 200 mg/L concentration on fresh leaves, neutral-pH

	Variable 1	*Variable 2*
Mean	44310.2	27541.6
Variance	8.64E+08	1.64E+08
Observations	5	5
Pearson Correlation	0.916812	
Hypothesized Mean Difference	0	
df	4	
t Stat	2.041597	
P(T<=t) one-tail	0.055371	
t Critical one-tail	2.131847	
P(T<=t) two-tail	0.110742	
t Critical two-tail	2.776445	

Table 2. Result of t-test for pixel count: paired samples of all 200 mg/L concentration, neutral-pH

	Variable 1	*Variable 2*
Mean	34559.5	23334.13
Variance	4.43E+08	2E+08
Observations	16	16
Pearson Correlation	0.393833	
Hypothesized Mean Difference	0	
df	15	
t Stat	2.221264	
P(T<=t) one-tail	0.021074	
t Critical one-tail	1.75305	
P(T<=t) two-tail	0.042147	
t Critical two-tail	2.13145	

Table 3. Result of t-test for cluster count: paired samples of 20 mg/L concentration on fresh leaves, neutral-pH

	Variable 1	*Variable 2*
Mean	1919.706	2138.647
Variance	440544.5	829883.9
Observations	17	17
Pearson Correlation	0.696186	
Hypothesized Mean Difference	0	
df	16	
t Stat	-1.37899	
P(T<=t) one-tail	0.093436	
t Critical one-tail	1.745884	
P(T<=t) two-tail	0.186872	
t Critical two-tail	2.119905	